TiO_2@Layered Double Hydroxide Core–Shell Nanospheres with Largely Enhanced Photocatalytic Activity Toward O_2 Generation

Yibo Dou, Shitong Zhang, Ting Pan, Simin Xu, Awu Zhou, Min Pu, Hong Yan, Jingbin Han, Min Wei,* David G. Evans, and Xue Duan*

TiO_2@CoAl-layered double hydroxide (LDH) core–shell nanospheres are fabricated via hydrothermal synthesis of TiO_2 hollow nanospheres followed by in situ growth of CoAl-LDH shell, which exhibit an extraordinarily high photocatalytic activity toward oxygen evolution from water oxidation. The O_2 generation rates of 2.34 and 2.24 mmol h^{-1} g^{-1} are achieved under full sunlight (>200 nm) and visible light (>420 nm), respectively, which are among the highest photocatalytic activities for oxygen production to date. The reason is attributed to the desirable incorporation of visible- light-active LDH shell with UV light-responsive TiO_2 core for promoted solar energy utilization. Most importantly, the combined experimental results and computational simulations reveal that the strong donor–acceptor coupling and suitable band matching between TiO_2 core and LDH shell facilitate the separation of photoinduced electron-hole pairs, accounting for the highly efficient photocatalytic performance. Therefore, this work provides a facile and cost-effective strategy for the design and fabrication of hierarchical semiconductor materials, which can be applied as photocatalyst toward water splitting and solar energy conversion.

1. Introduction

Recently, the harvesting of solar energy and conversion to clean and safe energy sources have evoked much attention owing to the decline in fossil-fuel production and increasing concern on environmental issues.[1–3] Since the pioneering work by Fujishima and Honda on water splitting to produce H_2 and O_2 under UV illumination utilizing TiO_2 photoelectrode,[4] numerous photocatalysts (e.g., ZnO, CdS, WO_3, and $SrTiO_3$) have been widely investigated for water splitting applications.[5–8] Despite a great deal of research, most developed photocatalysts are not appropriate for the visible-light-induced water splitting because of poor light utilization or weak photostability. In addition, the fast recombination rate of photoexcited electron–hole pairs generated by unfavorable band structure greatly limits their practical applications, which is an urgent problem to be solved as well.[9–11] Therefore, to satisfy the requirements of water splitting, the development of new materials or methodologies to obtain efficient photocatalysts with advantage of extended light response and an improved electron–hole separation efficiency remains a tremendous challenge.

In order to enhance the water splitting performance, an effective way is to build elaborate hybrid semiconductors with high efficiency of solar light utilization.[12–14] Recently, research interest on the nanostructured semiconductors is extended to 2D inorganic solids due to their large surface area and high photocatalytic efficiency.[15,16] Layered double hydroxides (LDHs) are 2D layered anionic clays generally expressed as $[M^{II}_{1-x}M^{III}_{x}(OH)_2](A^{n-})^{x/n}\cdot mH_2O$ (M^{II} and M^{III} are divalent and trivalent metals respectively, A^{n-} is interlayered anion).[17–20] Owing to their visible-light-response capability and large quantum yield, transition-metal-bearing LDH materials with semiconductor properties have attracted considerable attention as visible-light-induced photocatalysts.[21–23] However, pristine LDHs generally suffer from poor control over particle size, morphology as well as crystalline orientation, which restricts the efficiency of charge separation and photoconversion capability.[24,25] Taking into account the fact that TiO_2 nanocrystal can act as a good acceptor for photogenerated electrons,[1,5] the hybridization of TiO_2 with LDHs would provide an effective way to enhance the charge separation and photocatalytic efficiency. In this regard, the resulting heterostructure material would possess the following advantages: (i) prominent full sunlight utilization will be achieved owing to the combination of visible-light-active LDHs and UV-light-responsive TiO_2; (ii) the hierarchical structure enables a strong electronic coupling and convenient charge transfer at the interconnected interface, which would promote the separation of photoinduced electron–hole pairs.

In this work, TiO_2@CoAl-LDH core–shell nanospheres were prepared by a facile two-step route: hydrothermal synthesis of TiO_2 hollow nanospheres followed by in situ growth of CoAl-LDH shell (**Scheme 1**). The resulting material shows extremely

Y. Dou, S. Zhang, T. Pan, S. Xu, A. Zhou, Prof. M. Pu, Dr. H. Yan, Dr. J. Han, Prof. M. Wei, Prof. D. G. Evans, Prof. X. Duan
State Key Laboratory of Chemical Resource Engineering
Beijing University of Chemical Technology
Box 98, Beijing 100029, P.R. China
E-mail: hanjb@mail.buct.edu.cn;
weimin@mail.buct.edu.cn

DOI: 10.1002/adfm.201404496

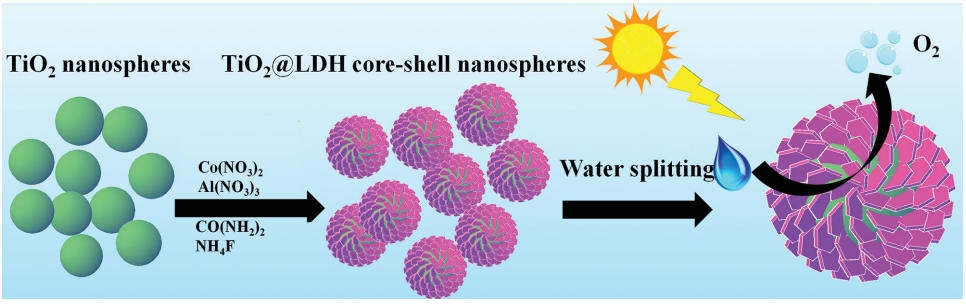

Scheme 1. A schematic illustration for the fabrication of TiO_2@CoAl-LDH core–shell nanospheres toward oxygen evolution from water splitting.

high photocatalytic activity toward oxygen evolution from water splitting, with O_2 generation rate of 2.34 and 2.24 mmol h^{-1} g^{-1} upon full sunlight and visible light illumination, respectively, which is the most effective photocatalyst for oxygen production to the best of our knowledge. The band structure matching between TiO_2 core and LDH shell plays a key role in the successful integration of these two individual compositions: the broad spectral response and strong electronic coupling between TiO_2 core and CoAl-LDH shell enable increased solar energy utilization and accelerated electron–hole separation, giving rise to a high photocatalytic activity toward oxygen production. In addition, the obtained TiO_2@CoAl-LDH photocatalyst exhibits excellent recyclability and stability, which can be potentially employed in a variety of photocatalysis areas including water splitting, photochemical devices and sensors.

2. Results and Discussion

TiO_2@CoAl-LDH nanospheres were prepared by a two-step process, which involoves the hydrothermal synthesis of TiO_2 hollow nanospheres as core followed by in situ growth of CoAl-LDH shell. **Figure 1** shows the XRD pattern of resulting TiO_2@CoAl-LDH, with pristine TiO_2 and CoAl-LDH as reference samples. The typical diffraction peaks at 2θ 25.28°, 38.04°, 48.05°, 53.89°, 55.06°, 62.69°, and 68.21° can be indexed to the (101), (004), (200), (105), (211), (204), and (116) reflections of an anatase TiO_2 (PDF-#89–4921) (curve a). For pure LDH nanoplatelets (curve b), the reflections at 2θ 12.18°, 24.31°, 35.96°, 39.15°, 47.22°, 61.22°, and 62.31° are attributed to the (003), (006), (009), (012), (018), (110), and (113) lattice planes of a hydrotalcite phase with CO_3^{2-} in the interlayer region (PDF-#51–0045). In the case of TiO_2@CoAl-LDH sample, a superimposition XRD pattern of TiO_2 and LDH is observed (curve c), which demonstrates the integration of these two compositions with high purity and good crystallization. In addition, the FT-IR spectra also display the existence of vibrational bands of TiO_2 and CoAl-LDH in the TiO_2@CoAl-LDH sample (Figure S1, Supporting Information), further confirming the formation of TiO_2@LDH heterostructure.

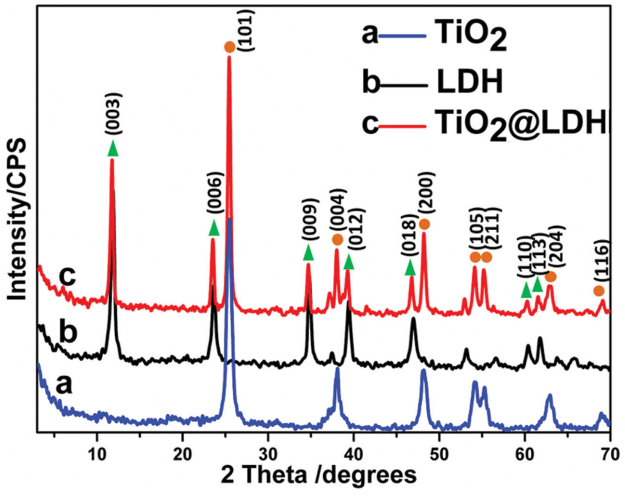

Figure 1. XRD patterns of a) TiO_2; b) CoAl-LDH; and c) TiO_2@CoAl-LDH sample.

The morphology and structure details of as-prepared TiO_2@LDH nanospheres were investigated by SEM and TEM observations. **Figure 2**A shows a typical SEM image of pristine TiO_2 nanospheres, which possess well-dispersed round shape with mean particle size of ≈250 nm (Figure S2, Supporting Information). Energy dispersive X-ray (EDX) spectroscopy analysis (Figure S3, Supporting Information) further reveals the existence of Ti and O element. TEM images confirm the hollow structure of TiO_2 nanospheres (Figure 2B), and the resolved interplanar distance of ≈0.35 nm is ascribed to the (101) plane of anatase TiO_2 (Figure 2C). After the in situ growth of CoAl-LDH shell, numerous nanoplatelets are observed with vertical orientation onto the TiO_2 core, giving rise to flower-like architecture (Figure 2D). The corresponding TEM image (Figure 2E) reveals a hollow core–shell structure with LDH shell thickness of ≈80 nm (Figure S4, Supporting Information). The high-resolution (HR) TEM image (Figure 2F) shows lattice fringes corresponding to the interplanar distance of ≈0.27 and ≈0.35 nm, which can be attributed to the (012) plane of CoAl-LDH phase (Figures S5 and S6, Supporting Information) and (101) plane of anatase TiO_2, respectively. Furthermore, EDX mapping analysis for an individual TiO_2@LDH nanosphere is shown in Figure 2G, in which Co, Al, and Ti are homogeneously distributed throughout the nanosphere. The EDX spectrum (Figure S7, Supporting Information) also shows the presence of Co, Al, and Ti, consistent with the mapping results. Therefore, the TiO_2@LDH core–shell heterostructure was obtained by grafting LDH nanoplatelets onto the surface of TiO_2 hollow nanospheres.

Time-dependent growth experiments were carried out to investigate the formation process of LDH shell onto TiO_2

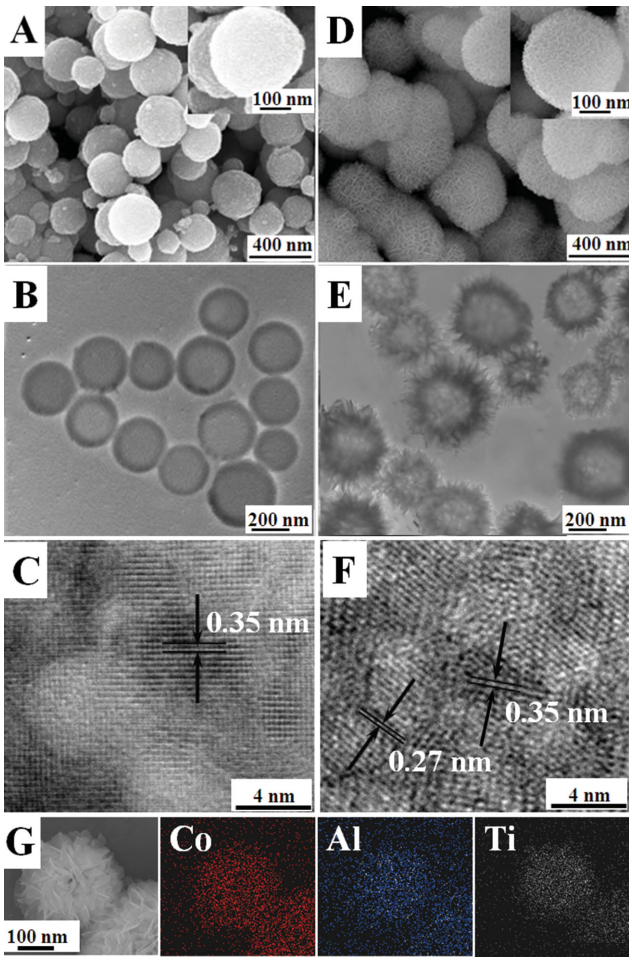

Figure 2. A) SEM, B) TEM, and C) HRTEM image of TiO_2 hollow nanospheres. D) SEM, E) TEM, and F) HRTEM image of TiO_2@LDH core–shell nanospheres. G) SEM image and EDX mapping for an individual TiO_2@LDH core–shell nanosphere.

nanospheres. A rough surface of TiO_2 nanopheres is found with the reaction time of 4 h (**Figure 3**A); numerous nanoplatelets come into formation on the TiO_2 nanospheres after 6 h (Figure 3B). As the reaction time increases to 10 h, a well-defined flower-like morphology with intercrossing LDH nanoplatelets is observed (Figure 3C). The XRD patterns of these samples are shown in Figure 3D. No obvious LDH phase can be observed for the sample with the reaction time of 4 h (curve a); while several reflections corresponding to LDH phase appear after 6 h (curve b), whose intensity increase significantly upon prolonging the growth time to 10 h (curve c). In addition, elemental analysis results based on EDX spectroscopy show the weight ratio of LDH in the TiO_2@LDH nanospheres is ≈4.4%, ≈15.5%, and ≈56.8% with the crystallization time of 4, 6, and 10 h, respectively, further indicating the gradual crystallization and growth of exterior LDH shell on TiO_2 core.

The surface area and porosity property are two important factors of photocatalysts for water splitting, which were investigated by N_2-adsorption/desorption measurements (**Figure 4**). In all cases (CoAl-LDH nanoplatelets, TiO_2 nanospheres and TiO_2@LDH nanospheres), typical IV isotherms with H3-type hysteresis loops ($P/P_0 > 0.4$) are observed, indicating the presence of mesopores in all the three samples. No obvious hysteresis loops is found for pristine CoAl-LDH sample, as a result of random aggregation of nanoplatelets; while TiO_2@LDH nanospheres display significant hysteresis loops without any limiting adsorption at high P/P_0 region, indicating the formation of slit-shaped pores formed by the stacking of LDH nanoplatelets on TiO_2 nanospheres. Specifically, the sample of TiO_2@LDH nanospheres possesses the maximum specific surface area (285.5 m^2 g^{-1}), much larger than that of hollow TiO_2 nanospheres (154.5 m^2 g^{-1}) and LDH nanoplatelets (63.8 m^2 g^{-1}). In addition, the pore size analysis based on the isotherms shows that these samples consist of a mesopore distribution in the range 2–5 nm. The high surface area and mesoporous feature of LDH@TiO_2 nanospheres would facilitate the exposure of active sites and promote their photocatalytic efficiency.

To better understand the interaction between CoAl-LDH shell and TiO_2 core, a fine-scan X-ray photoelectron spectroscopy (XPS) of the Co region was performed for the CoAl-LDH nanoplatelets and TiO_2@LDH nanospheres. For the CoAl-LDH sample, the binding energies at 781.3 and 797.3 eV correspond to Co $2p_{3/2}$ and Co $2p_{1/2}$, respectively (**Figure 5**A, curve a). The appearance of satellite peaks at 787.4 and 803.3 eV implies the presence of a high-spin divalent state of Co^{2+} in this sample. For the TiO_2@LDH nanospheres, however, the binding energies of Co $2p_{3/2}$ and Co $2p_{1/2}$ shift to 781.7 and 797.6 eV, respectively (Figure 5A, curve b). Concomitantly, the binding energies of Ti $2p_{3/2}$ and Ti $2p_{1/2}$ of TiO_2@LDH nanospheres exhibit a negative shift compared with those of pristine TiO_2 microspheres (Figure 5B). The increased and decreased binding energies of Co $2p$ and Ti $2p$ indicate an obvious electron transfer from LDH shell to TiO_2 core. The strong electronic coupling between LDH and TiO_2 would probably accelerate the electron–hole separation.

The photochemical activity of the semiconductors is particularly relevant with their optical absorption characteristics. In this regard, solid diffuse reflection of UV–vis spectrum (DRS) was carried out to investigate light response property of the photocatalysts. As shown in Figure 5C, TiO_2 hollow nanospheres display a steep absorption edge located at ≈380 nm assigned to the Ti–O bond;[26] while LDH nanoplatelets show a strong absorption capability in the visible light range. Consequently, the UV–vis spectrum of TiO_2@LDH core–shell nanospheres exhibit a significantly extended scale consisting of a visible light absorption band (400–800 nm) and an UV absorption band. The observed strong absorption toward visible light, relative to TiO_2 nanospheres, indicates the capability of TiO_2@LDH core–shell nanospheres as visible-light-active photocatalyst. Additionally, photoluminescence (PL) spectra are used to understand the efficiency of charge carrier capture, transfer, and migration of photocatalysts (Figure 5D), as PL emission arises from the recombination of free carriers.[26,27] TiO_2 nanospheres exhibit two emission peaks at ≈382 and ≈450 nm, which are attributed to the bandgap transition and the charge transfer transition of oxygen vacancy trapped electrons, respectively.[27] The pure LDH nanoplatelets show two obvious emission peaks at ≈355 and ≈460 nm, respectively. In contrast, a sharp decrease in PL behavior of TiO_2@LDH nanospheres is observed in comparison with pristine TiO_2 nanopheres and LDH nanoplatelets.

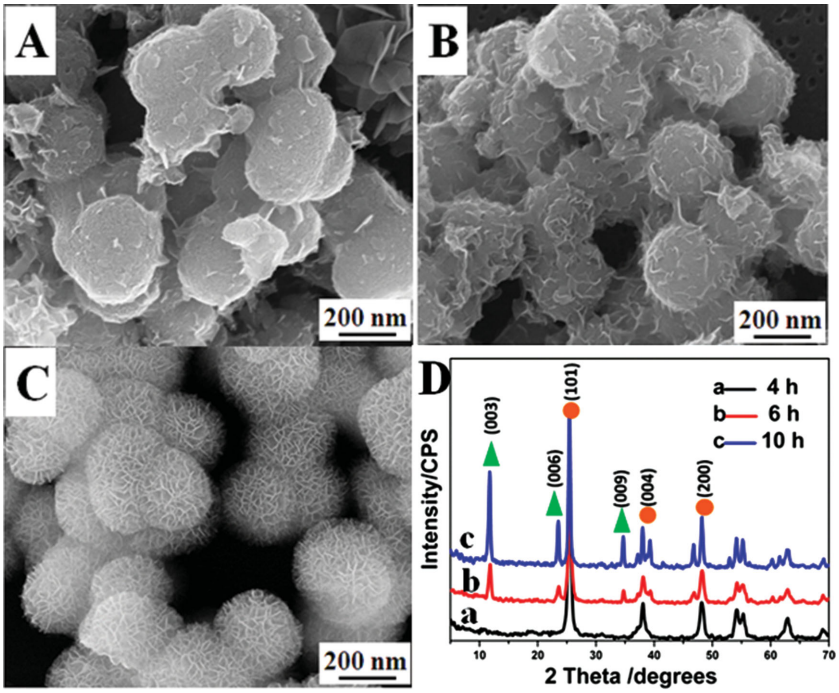

Figure 3. SEM images of TiO_2@LDH nanospheres synthesized with different reaction time: A) 4 h, B) 6 h, C) 10 h, and D) Corresponding XRD patterns of TiO_2@LDH nanospheres as a function of reaction time.

The nearly disappeared PL signal of TiO_2@LDH nanospheres indicates a largely depressed recombination of photoinduced electron–hole pairs in this heterostructure, which would promote the transfer efficiency of carrier and thus enhance the photocatalytic performance.

The photocatalytic activity toward water splitting over different samples was evaluated by monitoring the time-dependent production of O_2 in simulated-solar-light (λ > 200 nm) illuminated catalyst suspensions. As shown in **Figure 6**, TiO_2 nanospheres and LDH nanoplatelets display an O_2 generation rate of 0.27 and 0.98 mmol h^{-1} g^{-1}, respectively, owing to their poor light utilizations or probable high rate of charge recombination. In contrast, the TiO_2@LDH core–shell nanospheres exhibit an O_2 generation rate of 2.34 mmol h^{-1} g^{-1}, which is far superior to TiO_2 nanospheres and CoAl-LDH nanoplatelets. In addition, the control experiment shows the physical mixture of LDH/TiO_2 sample has weak oxygen generation ability (0.67 mmol h^{-1} g^{-1}) (Figure S8, Supporting Information). In order to make a systematic comparison with previous work, the photocatalytic activity of O_2 generation under visible light (λ>420 nm) was evaluated as well (Figure S9, Supporting Information). The O_2 generation rates of 2.24, 0.95, and 0.03 mmol h^{-1} g^{-1} is obtained for TiO_2@LDH, LDH, and TiO_2 sample, respectively. It should be noted that compared with previously reported photocatalysts,[3b,16,21,22b,23a,28–31] the TiO_2@LDH core–shell nanospheres in this work displays the highest photocatalytic O_2 generation rate under nearly the same experimental conditions (summarized in Table S1, Supporting Information). Moreover, the photocatalytic stability of TiO_2@LDH nanospheres was examined upon repeated photoreactions, and only a slight decrease in oxygen generation was observed after 10 cycles (Figure S10, Supporting Information). The SEM image (Figure S11, Supporting Information) shows no obvious change in its morphology after 10 cycles of photocatalytic reaction. The results demonstrate that TiO_2@LDH core–shell nanospheres can serve as a promising photocatalyst for oxygen evolution from water, with high activity and excellent recyclability.

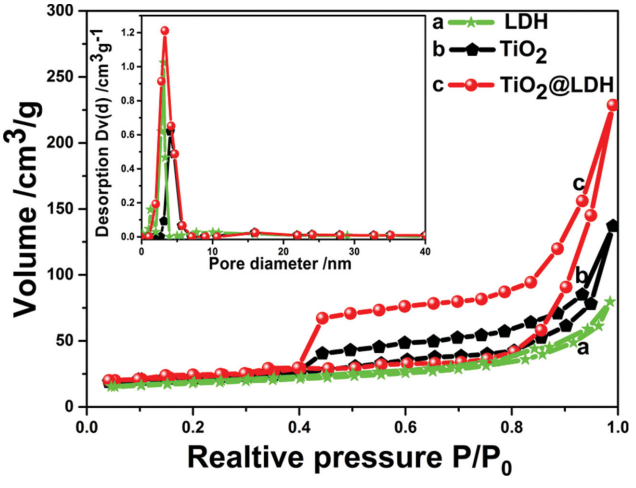

Figure 4. N_2 adsorption–desorption isotherms and pore size distributions (inset) of a) CoAl-LDH nanoplatelets; b) TiO_2 nanospheres; and c) TiO_2@LDH nanospheres, respectively.

To gain further insight into the electron–hole transport mechanism in the TiO_2@CoAl-LDH photocatalyst, density functional theory (DFT) + U calculations were carried out to elucidate the electronic structure of individual TiO_2 and LDH as well as their hybrid material from the theoretical viewpoint. The detailed information of model construction and computational method is described in the Supporting Information. After the optimization of TiO_2@LDH system, the average distance between the terminal oxygen atom in TiO_2 surface and the hydrogen atom in LDH surface is only 2.04 Å (**Figure 7**A); and the interaction energy between TiO_2 and LDH was calculated to be as low as −1.38 eV. Such low interaction energy combined with short distance between TiO_2 and LDH suggests the existence of pronounced hydrogen bond at their interface. Furthermore, Bader charge analysis[32] shows a significant charge transfer of 0.62 electron from LDH shell to TiO_2 core, leading to a substantial hole doping on the LDH, which is in accordance with the XPS experimental results (Figure 5A,B). The calculated density of states (DOS) curves indicate that both CoAl-LDH (Figures 7B, and S12) and TiO_2 (Figures 7C, and S13, Supporting Information) possess typical semiconductor characteristic, with bandgap measured from the valence band (VB) maximum to the conduction band (CB) minimum of 2.2 and 3.2 eV, respectively. It should be noted that, for a stable

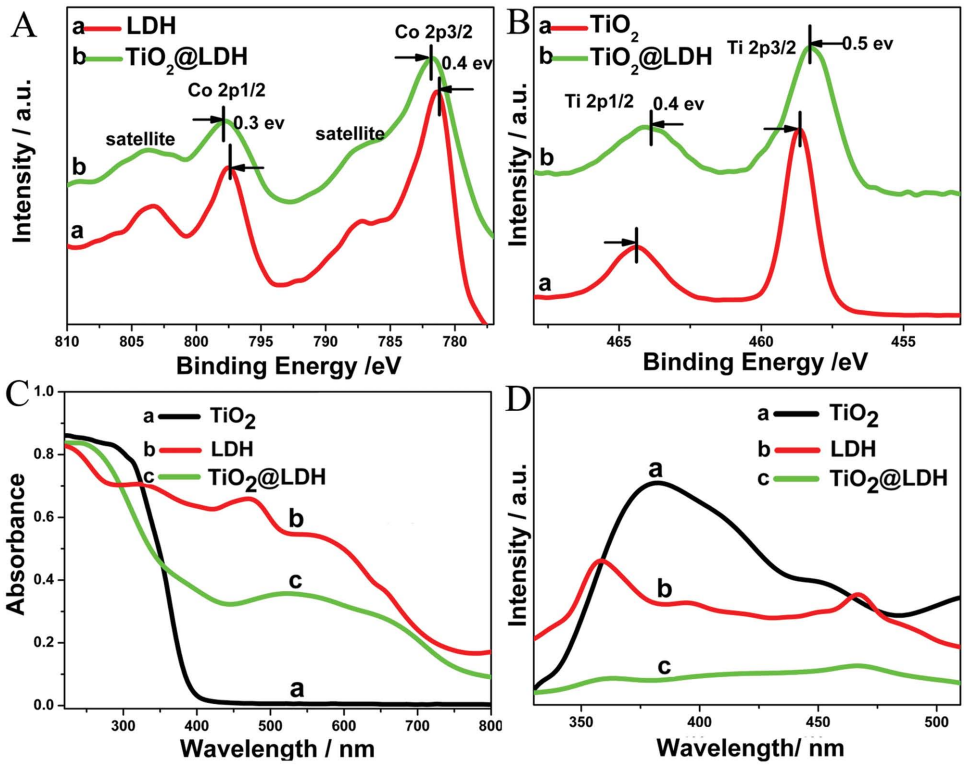

Figure 5. A) Co 2*p* and B) Ti 2*p* orbital XPS spectra of: a) LDH nanoplatelets and b) TiO_2@LDH nanospheres, respectively. C) UV–vis diffuse reflectance spectra and D) photoluminescence spectra of: a) TiO_2 nanospheres; b) LDH nanoplatelets; and c) TiO_2@LDH nanospheres, respectively.

TiO_2-LDH interface, the electronic structures of both TiO_2 and LDH exhibit a significant change, as a result of the strong donor–acceptor coupling at their interface. As shown in Figure 7D, the incorporation of CoAl-LDH induces the appearance of several peaks ascribed to Ti-3*d* orbital in the gap region of TiO_2, indicating the decrease of conduction band potential of TiO_2. The binding of TiO_2 in turn substantially narrows the bandgap of CoAl-LDH, giving rise to states occupied by Co-3*d* orbital in the gap region of LDH. In addition, the potential of unoccupied Ti-3*d* orbital is lower than that of empty Co-3*d* orbital. This implies that once the electrons are excited from the O-2*p* orbital in CoAl-LDH, they can inject into the CB of TiO_2, leaving a longer-lived hole in LDH. As a result, photoexcited electrons in the CB of LDH nanoplatelets could migrate into the unoccupied electronic level of TiO_2, leading to an efficient spatial separation of electrons and holes (Figure 7E). The resulting depression of electron–hole recombination is consistent with the remarkably decreased photoluminescence signal after hybridization (Figure 5D), as previously discussed. Therefore, the sophisticated core–shell structure of TiO_2@LDH nanospheres with strong donor–acceptor coupling and favorable band matching facilitate the charge separation and consequently induce highly efficient generation of O_2.

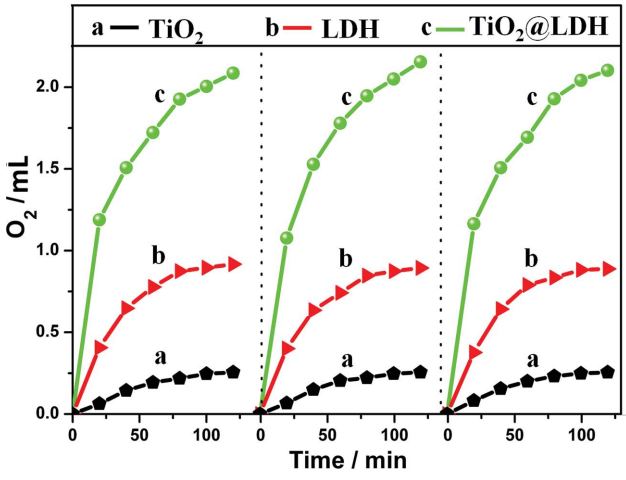

Figure 6. Volume of O_2 generation as function of irradiation time (λ > 200 nm) in three consecutive cycles for a) TiO_2 nanospheres; b) CoAl-LDH nanoplatelets; c) TiO_2@LDH nanospheres, respectively.

3. Conclusion

In summary, we demonstrate the fabrication of TiO_2@LDH core–shell heterostructure by a facile in situ growth of LDH shell onto the surface of TiO_2 hollow nanospheres, which exhibits significantly enhanced photocatalytic behavior for O_2 generation, including extraordinarily high rate of evolution, excellent recyclability, and stability. This can be ascribed to the increased solar energy absorption capability of TiO_2@LDH system by integrating visible-light-active LDH with UV-light-responsive TiO_2. Most importantly, the strong electronic coupling and suitable band matching between LDH and TiO_2 confirmed by both experimental investigation and

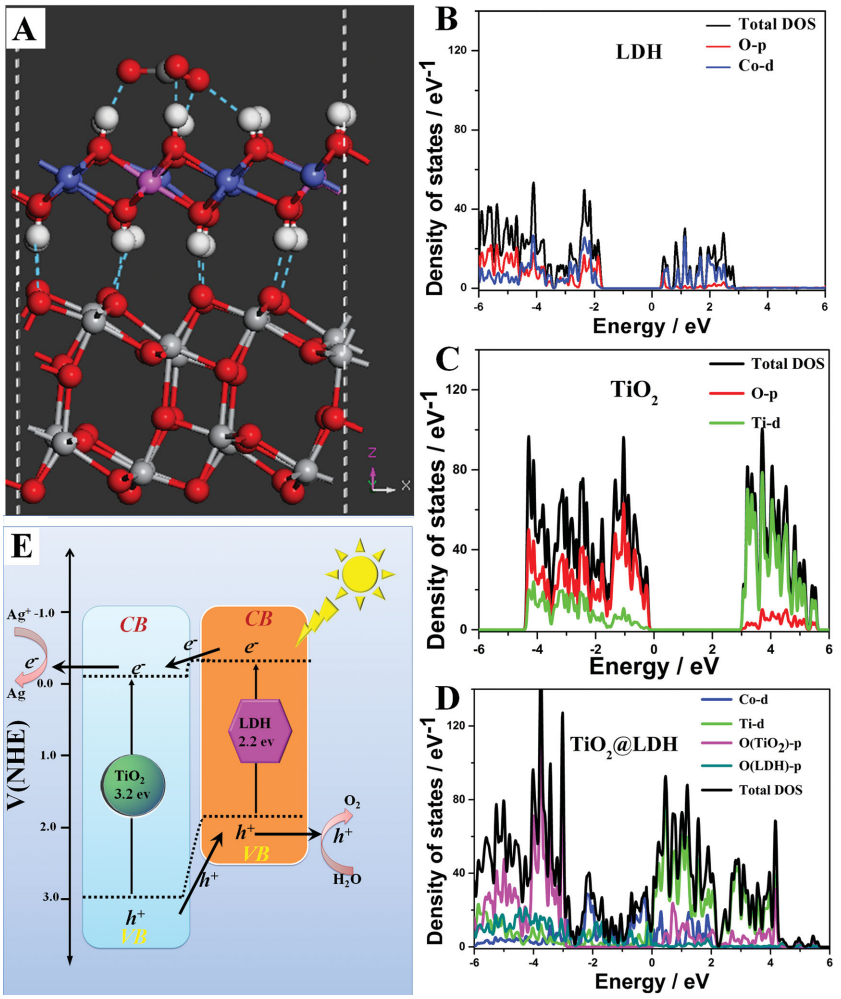

Figure 7. A) The optimized geometry of TiO_2@CoAl-CO_3-LDH model (white, H; red, O; pink, Al; green, C; blue, Co; and grey, Ti). The density of states for B) LDH slab model; C) TiO_2 (101) surface model; and D) TiO_2@CoAl-LDH system, respectively. Fermi level was aligned to the vacuum level. E) A schematic illustration of photoexcited electron transfer and oxygen generation over the TiO_2@CoAl-LDH system.

computational simulation further accelerate the separation of photoinduced electron–hole pairs. To the best of our knowledge, the TiO_2@LDH hybrid material displays the highest oxygen generation rate among the reported photocatalysts toward water oxidation. It is expected that the synthetic strategy in this work can be extended to the preparation of other hierarchical structures with enhanced performances in photocatalysis and energy conversion.

4. Experimental Section

Synthesis of TiO_2 Hollow Nanospheres: Anatase TiO_2 hollow nanospheres were synthesized based on the previously reported method.[33,34] Briefly, tetrabutyl titanate (2 mL) and ethanol (25 mL) was dropped into deionized water (100 mL) under vigorous stirring. Then, $NaHCO_3$ solution (0.25 M, 50 mL) was added into the previous solution drop by drop. The resulting solution was transferred to a Teflon-lined stainless-steel autoclave and heated at 180 °C for 48 h. After the autoclave was cooled to room temperature, the resulting white precipitate was washed thoroughly with anhydrous ethanol and dried in vacuum at 60 °C for 12 h.

Synthesis of TiO_2@LDH Core–Shell Nanospheres: An in situ crystallization of CoAl-LDH nanoplatelets shell on the surface of TiO_2 hollow nanospheres was carried out by the following procedure: $Co(NO_3)_2{\cdot}6H_2O$ (15 mmol), $Al(NO_3)_3{\cdot}9H_2O$ (5 mmol), urea (50 mmol), and NH_4F (20 mmol) were dissolved in deionized water to form a solution with a total volume of 70 mL. The TiO_2 hollow nanospheres (10 mmol) were dispersed in the above solution under vigorous stirring and transferred to a Teflon-lined stainless-steel autoclave at 100 °C for 10 h. Finally, the resulting TiO_2@LDH core–shell nanospheres were washed with water and anhydrous ethanol thoroughly, and then dried in vacuum at 60 °C for 12 h.

Synthesis of CoAl-LDH Nanoplatelets: The CoAl-LDH nanoplatelets as a reference sample were prepared by a hydrothermal method reported by our group.[35] Typically, 100 mL of solution A ($Al(NO_3)_3{\cdot}9H_2O$: 0.10 M and $Co(NO_3)_2{\cdot}6H_2O$: 0.20 M) and 100 mL of solution B (urea: 1.0 M) were mixed together. The mixed solution was transferred into a Teflon-lined stainless steel autoclave and hydrothermally treated at 110 °C for 24 h. The resulting LDH slurry was obtained via centrifugation, washed thoroughly and dried in vacuum at 60 °C for 12 h.

Oxygen Generation from Water Splitting: The photocatalytic reaction was performed in a Pyrex glass cell with a stationary temperature at 50 °C, which was connected with a closed gas circulation system. The photocatalyst (LDH nanoplatelets, TiO_2 hollow nanospheres or TiO_2@LDH nanospheres) (0.02 g) was suspended individually in an aqueous solution (100 mL) containing $AgNO_3$ (0.01 g) as a sacrificial reagent. The suspension was then thoroughly degassed and irradiated using a Xe lamp (300 W). The amount of oxygen generation was analyzed at given time intervals using an online gas chromatograph (GC-7890II; Techcomp. Co., Ltd). The activity of different photocatalysts was determined on the basis of the average rate of O_2 generation at least 5 cycles.

Sample Characterization: Powder X-ray diffraction patterns of the samples were collected on a Shimadzu XRD-6000 diffractometer using a Cu Kα source, with a scan step of 0.02° and a scan range between 3° and 70°. X-ray photoelectron spectroscopy (XPS) measurements were performed using an ESCALAB 250 instrument (Thermo Electron) with Al Kα radiation. The morphology of the samples was investigated using a scanning electron microscope (SEM; Zeiss SUPRA 55) with an accelerating voltage of 20 kV, combined with energy dispersive X-ray (EDX) spectroscopy for the elemental analysis. Transmission electron microscopy (TEM) images were recorded with Philips Tecnai 20 and JEOL JEM-2010 high-resolution transmission electron microscopes. The accelerating voltage was 200 kV in each case. The specific surface area determination and pore size analysis were performed by Brunauer–Emmett–Teller (BET) and Barrett–Joyner–Halenda (BJH) methods, respectively, using a Quantachrome Autosorb-1C-VP Analyzer. Prior to the measurements, the samples were degassed at 120 °C for 10 h. The fluorescence spectra were recorded on a Shimadzu RF-5301PC spectrofluorometer and both the excitation and emission slits were 3.0 nm. The Fourier transform infrared (FT-IR) spectra were obtained using a Vector 22 (Bruker) spectrophotometer with 2 cm^{-1} resolution. A Shimadzu U-3000 spectrophotometer was applied to collect the solid diffuse reflection spectrum in the range of 200–800 nm.

Supporting Information

Supporting Information is available from the Wiley Online Library or from the author.

Acknowledgements

This work was supported by the 973 Program (Grant No. 2014CB932102), the National Natural Science Foundation of China (NSFC), the Beijing Natural Science Foundation (Grant No. 2132043), and the Fundamental Research Funds for the Central Universities (Grant No. YS1406). M. Wei particularly appreciates the financial aid from the China National Funds for Distinguished Young Scientists of the NSFC. We acknowledge National Supercomputing Center in Shenzhen for providing the computational resources and materials studio (version 6.1, CASTEP module).

Received: December 18, 2014
Revised: February 8, 2015
Published online: February 25, 2015

[1] a) N. S. Lewis, *Science* **2007**, *315*, 798; b) X. Long, J. Li, S. Xiao, K. Yan, Z. Wang, H. Chen, S. Yang, *Angew. Chem. Int. Ed.* **2014**, *53*, 1; c) B. O'Regan, M. Grätzel, *Nature* **1991**, *353*, 737.

[2] a) E. Chornet, S. Czernik, *Nature* **2002**, *418*, 928; b) X. Ge, L. Chen, L. Zhang, Y. Wen, A. Hirata, M. Chen, *Adv. Mater.* **2014**, *26*, 3100.

[3] a) Y. D. Yin, F. Kim, Y. Q. Yan, *Adv. Mater.* **2003**, *15*, 353; b) X. B. Chen, S. H. Shen, L. J. Guo, S. S. Mao, *Chem. Rev.* **2010**, *110*, 6503.

[4] A. Fujishima, K. Honda, *Nature* **1972**, *238*, 37.

[5] a) A. Mukherji, R. Marschall, A. Tanksale, C. Sun, S. Smith, G. Lu, L. Wang, *Adv. Funct. Mater.* **2011**, *21*, 126; b) Z. Zou, J. Ye, K. Sayama, H. Arakawa, *Nature* **2001**, *414*, 625.

[6] A. Kudo, Y. Miseki, *Chem. Soc. Rev.* **2009**, *38*, 253.

[7] A. Testino, I. R. Bellobono, V. Buscaglia, C. Canevali, M. D'Arienzo, S. Polizzi, R. Scotti, F. Morazzoni, *J. Am. Chem. Soc.* **2007**, *129*, 3564.

[8] X. Chen, S. S. Mao, *Chem. Rev.* **2007**, *107*, 2891.

[9] T. Yeh, J. Syu, C. Cheng, T. Chang, H. Teng, *Adv. Funct. Mater.* **2010**, *20*, 2255.

[10] X. F. Gao, W. T. Sun, Z. D. Hu, G. Ai, Y. L. Zhang, S. Feng, F. Li, L. M. Peng, *J. Phys. Chem. C* **2009**, *113*, 20481.

[11] a) C. Cox, M. Winkler, J. Pijpers, T. Buonassisi, D. Nocera, *Energy Environ. Sci.* **2013**, *6*, 532; b) G. Xie, K. Zhang, B. Guo, Q. Liu, L. Fang, J. Gong, *Adv. Mater.* **2013**, *25*, 3820.

[12] a) Z. Y. Liu, D. D. Sun, P. Guo, J. O. Leckie, *Nano Lett.* **2007**, *7*, 1081; b) A. Iwase, Y. H. Ng, Y. Ishiguro, A. Kudo, R. Amal, *J. Am. Chem. Soc.* **2011**, *133*, 11054.

[13] a) M. G. Walter, E. L. Warren, J. R. McKone, S. W. Boettcher, Q. Mi, E. A. Santori, N. S. Lewis, *Chem. Rev.* **2010**, *110*, 6446; b) J. Z. Zhang, *MRS Bull.* **2011**, *36*, 48; c) T. Jaramillo, S. Baeck, A. Shwarsctein, K. Choi, G. Stucky, E. Mcfarland, *J. Comb. Chem.* **2005**, *7*, 264.

[14] a) Y. H. Lu, S. P. Russo, Y. P. Feng, *Phys. Chem. Chem. Phys.* **2011**, *13*, 15973; b) R. Abe, M. Higashi, K. Domen, *J. Am. Chem. Soc.* **2010**, *132*, 11828.

[15] M. Shao, F. Ning, M. Wei, D. G. Evans, X. Duan, *Adv. Funct. Mater.* **2014**, *24*, 580.

[16] J. L. Gunjakar, I. Y. Kim, J. M. Lee, N. S. Lee, S. J. Hwang, *Energy Environ. Sci.* **2013**, *6*, 1008.

[17] a) Q. Wang, D. O'Hare, *Chem. Rev.* **2012**, *112*, 4124; b) D. Yan, J. Lu, M. Wei, S. Qin, L. Chen, S. Zhang, D. G. Evans, X. Duan, *Adv. Funct. Mater.* **2011**, *21*, 2497; c) L. Li, R. Ma, Y. Ebina, N. Iyi, T. Sasaki, *Chem. Mater.* **2005**, *17*, 4386; d) S. Mitchell, T. Biswick, W. Jones, G. Williams, D. O'Hare, *Green Chem.* **2007**, *9*, 373.

[18] a) A. M. Fogg, V. M. Green, H. G. Harvey, D. O'Hare, *Adv. Mater.* **1999**, *11*, 1466; b) G. R. Williams, D. O'Hare, *J. Mater. Chem.* **2006**, *16*, 3065; c) G. R. Williams, T. G. Dunbar, A. J. Beer, A. M. Fogg, D. O'Hare, *J. Mater. Chem.* **2006**, *16*, 1231; d) S. Mitchell, I. R. Baxendale, W. Jones, *Green Chem.* **2008**, *10*, 629; e) H. C. Greenwell, W. Jones, D. N. Stamires, P. O'Connord, M. F. Brady, *Green Chem.* **2006**, *8*, 1067.

[19] a) M. C. Richardson, P. S. Braterman, *J. Phys. Chem. C* **2007**, *111*, 4209; b) J. W. Bocair, P. S. Braterman, *Chem. Mater.* **1999**, *11*, 298; c) A. Illaik, C. Taviot-Guého, J. Lavis, S. Commereuc, V. Verney, F. Leroux, *Chem. Mater.* **2008**, *20*, 4854; d) S. Gago, T. Costa, J. S. de Melo, I. S. Gonçalves, M. Pillinger, *J. Mater. Chem.* **2008**, *18*, 894; e) A. W. Myong, M. S. Song, T. W. Kim, I. Y. Kim, J. Y. Ju, Y. S. Lee, S. J. Kim, J. H. Choy, S. J. Hwang, *J. Mater. Chem.* **2011**, *21*, 4286.

[20] a) B. Monteiro, S. Gago, F. A. A. Paz, R. Bilsborrow, I. S. Gonçalves, M. Pillinger, *Inorg. Chem.* **2008**, *47*, 8674; b) F. Leroux, C. Taviot-Guého, *J. Mater. Chem.* **2005**, *15*, 3628; c) W. Shi, S. He, M. Wei, D. G. Evans, X. Duan, *Adv. Funct. Mater.* **2010**, *20*, 3856.

[21] C. G. Silva, Y. Bouizi, V. Fornes, H. Garcia, *J. Am. Chem. Soc.* **2009**, *131*, 13833.

[22] a) W. B. Joseph, S. B. Paul, J. Jiang, S. Lou, F. Yarberry, *Chem. Mater.* **1999**, *11*, 303; b) J. L. Gunjakar, T. W. Kim, H. N. Kim, I. Y. Kim, S. J. Hwang, *J. Am. Chem. Soc.* **2011**, *133*, 14998; c) S. Cho, J. Jang, K. Kong, E. Kim, K. Lee, J. Lee, *Adv. Funct. Mater.* **2013**, *23*, 2348.

[23] a) Y. Lee, J. Choi, H. Jeon, K. Choi, J. Lee, J. Kang, *Energy Environ. Sci.* **2011**, *4*, 914; b) F. E. Osterloh, *Chem. Mater.* **2008**, *20*, 35; c) K. Parida, M. Satpathy, L. Mohapatra, *J. Mater. Chem.* **2012**, *22*, 7350.

[24] Y. Zhao, P. Chen, B. Zhang, D. Su, S. Zhang, L. Tian, J. Lu, Z. Li, X. Cao, B. Wang, M. Wei, D. G. Evans, X. Duan, *Chem. Eur. J.* **2012**, *18*, 11949.

[25] a) B. Li, Y. Zhao, S. Zhang, W. Gao, M. Wei, *ACS Appl. Mater. Interfaces* **2013**, *5*, 10233; b) K. Parida, L. Mohapatra, *Dalton Trans.* **2012**, *41*, 1173.

[26] W. Zhou, H. Liu, J. Wang, D. Liu, G. Du, J. Cui, *ACS Appl. Mater. Interfaces* **2010**, *2*, 2385.

[27] J. Tian, Y. Sang, Z. Zhao, W. Zhou, D. Wang, X. Kang, H. Liu, J. Wang, S. Chen, H. Cai, H. Huang, *Small* **2013**, *9*, 3864.

[28] a) E. Borgarello, J. Kiwi, M. Grätzel, E. Pelizzetti, M. Visca, *J. Am. Chem. Soc.* **1982**, *104*, 2996; b) H. Kato, A. Kudo, *J. Phys. Chem. B* **2002**, *106*, 5029; c) H. G. Kim, O. S. Becker, J. S. Jang, S. M. Ji, P. H. Borse, J. S. Lee, *J. Solid State Chem.* **2006**, *179*, 1214; d) H. G. Kim, D. W. Hwang, J. S. Lee, *J. Am. Chem. Soc.* **2004**, *126*, 8912.

[29] a) Y. Miseki, H. Kusama, H. Sugihara, K. Sayama, *J. Phys. Chem. Lett.* **2010**, *1*, 1196; b) A. Kudo, K. Omori, H. Kato, *J. Am. Chem. Soc.* **1999**, *121*, 11459; c) Y. Hosogi, H. Kato, A. Kudo, *J. Mater. Chem.* **2008**, *18*, 647.

[30] a) H. G. Kim, E. D. Jeong, P. H. Borse, S. Jeon, K. Yong, J. S. Lee, W. Li, S. H. Oh, *Appl. Phys. Lett.* **2006**, *89*, 064103; b) Á. Valdés, Z. Qu, G. Kroes, *J. Phys. Chem. C* **2008**, *112*, 9872.

[31] X. Cui, Y. Wang, G. Jiang, Z. Zhao, C. Xu, Y. Wei, A. Duan, J. Liu, J. Gao, *RSC Adv.* **2014**, *4*, 15689.

[32] E. Sanville, S. D. Kenny, R. Smith, G. J. Henkelman, *Comput. Chem.* **2007**, *28*, 899.

[33] a) J. Zhang, Z. Zhu, Y. Tang, X. Feng, *J. Mater. Chem. A.* **2013**, *1*, 3752; b) G. Yang, P. Hu, Y. Cao, F. Yuan, R. Xu, *Nanoscale Res. Lett.* **2010**, *5*, 1437.

[34] a) H. Yang, H. Zeng, *J. Phys. Chem. B* **2004**, *108*, 3492; b) S. Wang, Y. Ding, S. Xu, Y. Zhang, G. Li, L. Hu, S. Dai, *Chem. Eur. J.* **2014**, *20*, 4916.

[35] Y. Dou, S. Xu, X. Liu, J. Han, H. Yan, M. Wei, D. G. Evans, X. Duan, *Adv. Funct. Mater.* **2014**, *24*, 514.